Compact low-cost unit for photometric testing of automotive headlamps

S. Royo, MEMBER SPIE
M. J. Arranz
J. Arasa, MEMBER SPIE
Technical University of Catalonia (UPC-CD6)
Centre for Sensor, Instrument and
Systems Development
Rambla de Sant Nebridi 10
08222 Terrassa, Spain
E-mail: royo@oo,upc.edu

M. Cattoen
T. Bosch
ENSEEIHT
2 Rue Charles Camichel
BP7122 31071
Toulouse CEDEX 7, France

Abstract. A novel proposal for low-cost photometric testing of automotive headlamps is presented, using a combination of well-known optical metrology principles. Deflectometric measurement techniques and CCD-based photometry permit the precise measurement of the energy distribution and the direction of propagation on a plane close to the headlamp, while simple image-processing techniques permit the far-field photometric distribution on a distant plane to be reconstructed from the near-field data measured. The setup constructed and the main calibrations involved are presented, and results for different headlamp models are shown. The technique may be applied to light sources other than headlamps in order to calculate far-field distributions on any predefined surface of interest from near-field measurements. © *2006 Society of Photo-Optical Instrumentation Engineers.* [DOI: 10.1117/1.2213622]

1 Introduction

At a time when mortality and morbidity problems linked to the mobility of citizens are one of the main concerns in industrialized countries, driving at night is still dangerous. Despite all technological advances, it has been shown that similar numbers of deaths in traffic accidents occur during the day and at night, although at night only 25% of the traffic is on the road.[1] This fact has led to different technological improvements, including the development of night-vision systems for automobiles,[2] which, at present, are mostly addressed to high-end vehicles. Automotive lighting and headlamps in particular are still the most effective aid for the majority of drivers at night, including coach and truck drivers.

Current commercial headlamps are complex-shaped extended light sources that must comply with a series of requirements, both in passing- and in driving-beam conditions. Specific regulations governing the photometric distribution that must be attained exist in different regions of the world, by which headlamps are classified into different categories (symmetrical, asymmetrical, sealed beam, gas discharge, etc.).[3–5] These tests, for all headlamp types, involve the measurement of the photometric distribution of the headlamps in far-field conditions, usually on a plane at a distance of 25 m from the headlamps and orthogonal to the direction of the vehicle. Such tests are carried out in photometric tunnels, which are specially designed facilities in which the headlamp is placed on a mechanical goniometer and its distribution is measured by a high-accuracy photometer at the other end of the tunnel. Such facilities are rare, expensive to rent, and usually far away from the de-

signer's or manufacturer's facilities. At a time when new headlamp designs and sources are put onto the market in quick succession, it is essential to reduce the number of times the photometric tunnel is used to validate new headlamp designs.

Different approaches to the problem have been proposed in several patents,[6,7] which is an indication of the technological relevance of the problem. Some of these patents have managed to reach the market, for both headlamp validation and alignment. A common way of reducing visits to the photometric tunnel and even of carrying out alignment testing on the quality-control workbench has been to reduce the length of the instrument by placing the headlamp at the focal point of a large-diameter positive lens (either refractive or Fresnel-type), in order to measure the projected energy distribution on a nearby screen. The critical alignment of the headlamp behind the lens and the uncontrolled effect of the aberrations of the lens (mainly distortion) on the photometric distribution obtained are the main drawbacks of this so-called *reduced workbench* approach. Other approaches, such as compact goniometers, are very expensive due to their mechanical complexity.

In this paper, we present a new, cost-effective technique based on sampling the near-field energy distribution using a combination of deflectometric and photometric techniques, which make it possible to quantify the amount of energy traveling in each direction, using a calibrated CCD camera as a light-sensing unit. Image-processing techniques can then be used to reconstruct the photometric distribution on any surface, and specifically on a plane at a distance of 25 m. The measurement procedure, however, would enable the photometric distribution to be determined for a surface at any distance, and the unit developed could also be used
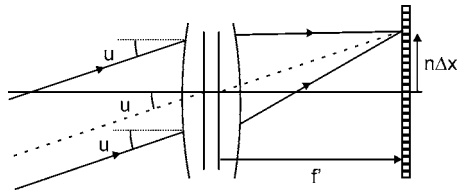
Fig. 1 CCD sensor configured as a slope mapper: lens focused at infinity means that each pixel only receives the rays arriving from a given propagation direction.

to characterize other types of light sources, such as luminaires, LEDs, or automotive side and tail lights, using the same measurement principle with small adjustments in the sensor (if necessary).

The paper is divided into five sections in addition to this Introduction. In Sec. 2 the main features of the measurement principle are presented, and Sec. 3 is devoted to the presentation of the setup built for the unit and to the description of the calibrations needed for the sensor's proper functioning. Section 4 describes the theoretical model and experimental setups used for the photometric calibration of the unit, and Sec. 5 presents the far-field photometric distributions measured with the unit for an asymmetrical and a symmetrical headlamp. These measurements are compared with reference measurements performed in a 25-m photometric tunnel where photometric validation tests of commercial headlamps are performed daily. Section 6 sums up the main conclusions of the work.

2 Measurement Principle

The development of a compact unit relies on an accurate measurement strategy in near-field conditions, which permits a precise calculation of the illumination pattern in far-field conditions. A combination of deflectometric techniques, which are used to measure the direction of the energy, and CCD-based photometric techniques, which are used to quantify the amount of energy propagating in each direction, was chosen for near-field sensing. The complete near-field energy distribution is then obtained by moving the sensor across a measurement plane placed close to the headlamp, at a fixed distance of several centimeters, typically 20 cm. From these data, a classical geometrical projection technique yields the desired far-field photometric distribution on the desired final surface. These three procedures are briefly analyzed below.

Deflectometric techniques assume that the geometrical optics approximation is valid for sampling luminance fields as light rays traveling in space. One of the metrological approaches involves sampling the direction of the propagating energy with a CCD camera through a lens focused at infinity.[8] Under these conditions, a pixel with order numbers n, m in the CCD array receives the bundle of rays with average slopes (Fig. 1) that are given by

$$\tan u = n \frac{\Delta x}{f'},$$

$$\tan v = m \frac{\Delta y}{f'}, \tag{1}$$

where we have assumed the directions of the rows (columns) of the CCD aligned along the X (Y) axes, and where u (v) is the angle determining the slope of the ray along the X (Y) axis, Δx (Δy) the size of the pixel along the X (Y) axis, and f' the focal length of the lens. Under these working conditions, the CCD array becomes a slope mapper of the incoming wavefront. With the experimental setup presented in this paper, the linear approximation for slope measurement will remain valid for all the measurements.

Using this arrangement, while the position of the pixel in the CCD array measures the direction of luminous energy propagation, the gray level of the same pixel can simultaneously measure how much energy is propagating in that particular direction.[9] This approach relies on three key points: (a) having a sensor with a spectral response equaling the CIE V_λ photopic curve to perform accurate photometric measurements; (b) ensuring a reliable vignetting and distortion correction to compensate accurately for possible energy losses or ray deviations at edge of field caused by the optical system or mounts; and (c) ensuring a dynamic range that is as linear and as extended as possible to avoid saturating the signal, without losing accuracy. All these issues are discussed in detail in Sec. 3, with a number of additional factors to be considered in CCD calibrations that are discussed in the literature,[10] such as the number of digitization bits or pixel response nonuniformity.

Using the sensing strategy proposed, each register on the CCD array contains information on the energy distribution and propagation direction at the aperture of the lens. Then, by moving the sensor over a set of given points (x_m, y_m) on a measurement plane close to the source to obtain the register of the luminance field at each of these points, the complete near-field energy pattern may be sensed. To obtain the final photometric distribution in the far field, simply projecting the energy contained in the near-field registers onto the desired final surface enables a complete reconstruction of the far-field distribution. In this paper, the final surface is considered to be a plane, to allow comparison with measurements in a photometric tunnel, although curved surfaces at arbitrary positions simulating traffic signs, roads, cars illuminated from behind, etc., may be used to project the near-field pattern onto them.

3 Setup

Two different parts of the unit may be distinguished, which correspond to the mechanical displacements for the sensor and the sensor itself.

3.1 Mechanical Setup

A complete motorized mechanical setup with self-designed control electronics and a test user interface was designed and built to position the sensor accurately and repetitively at the array of points (x_m, y_m) required. Two stepping motors connected to high-accuracy encoders demonstrated accuracies and repeatabilities in the displacement of 10 μm. The distribution is captured onto a plane for simplicity's sake; preliminary tests showed that the inclusion of additional degrees of freedom did not significantly improve far-
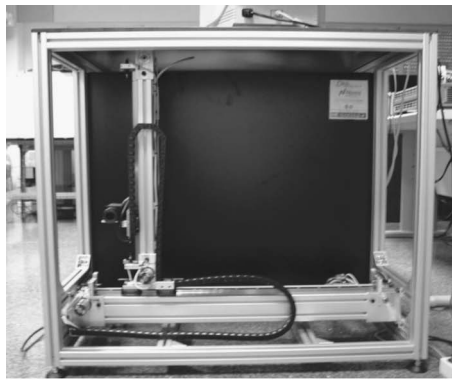
(a)

(b)

Fig. 2 Mechanical setup: (a) complete; (b) detail of vertical axis and sensor.

field photometric measurements. Figure 2 shows two pictures of the mechanical setup built for this purpose.

3.2 Sensor

In the sensor we may distinguish between the optical system, which includes filters, mounts, and the camera lens, and the CCD camera and electronics involved in image acquisition. A 17.2-mm-focal-length commercial lens with negligible distortion at edge of field (below 0.5%, about one pixel, at the edge of the CCD sensor) and a large working aperture ($N=1.7$) was selected. Two sets of filters were placed in front of this lens in an external mount fixed to the lens structure. On one side, an equalizing filter plus a photopic filter yielded the spectral response of the sensor close to the photopic curve of the eye. On the other side, a group of neutral filters with flat spectral response were used in order to adjust the radiance levels up to a point at which the camera was not saturated at the minimum exposure time.

The camera selected was a 2/3-in. CCD camera with external shutter control. The shutter was controlled using self-developed electronics, in order to automatically adjust the optimum shutter value and thus prevent the saturation of the signal. This allowed a significant extension of the

dynamic range of the system. The camera and digitizer used provided one 8-bit image at each measurement point, which was saved onto the computer's hard disk. Although some commercially available systems provided a greater number of digitization bits, this feature increased the cost of the unit considerably. The lower number of digitization bits was partially compensated for by using an externally controlled shutter. The dark-field signal of the camera was determined and subtracted from all the registers. The photoresponse nonuniformity of the CCD array was measured and found to be negligible.

The spectral response of the final sensor (camera+lens +filters) was then accurately measured by comparing the response of the sensor in gray levels with a number of calibrated radiance values at different wavelengths, from 480 to 690 nm in 10-nm intervals. Figure 3(a) plots the spectral response curve of our sensor (symbols) besides the standard CIE photopic curve (line), showing very good agreement. The results of computing the difference between the spectral response of our sensor and the photopic V_λ curve yielded an f_1' value[11] of 4.6%, which is not enough for it to be classified as an optimum-quality photometric detector (this would require f_1' values below 3%), although it is more than enough for the sensor to be considered a good-quality photometric detector ($f_1' < 8\%$). This value could easily be enhanced by using a filter exactly matched to the spectral response of the CCD array, instead of a combination of an equalizing and a commercial photopic filter.

An important verification regarding sensor performance involved testing the linearity of the response over the complete dynamic range, and the shutter law for the photometric compensation of the energy values registered under different illumination conditions. This was especially important because of the dynamic adjustment of the shutter: each shutter value corresponds to a different exposure time of the sensor. In order to test the complete response of the unit, a LED was placed in front of the sensor, and its emission was controlled through the circulating intensity. The sensor acquired the images at different intensities, while ensuring that no saturation occurred, and registered the average gray level obtained for a shutter value x comprised within the range $[0, 255]$. The system yielded high linearity ($r^2=0.9999$), as may be seen in Fig. 3(b), and gave a shutter law

$$L = (7.26 \pm 0.01)x + (3.3 \pm 1.1), \qquad (2)$$

where L is the gray-level value obtained from the sensor and x the shutter value. With this approach we may change the exposure time depending on the illumination of each register to maximize the number of discriminated gray levels per register while at the same time we avoid saturation. The shutter law is used to correct the energy measurement according to the exposure value x used. The number of discriminated gray levels when the external shutter adjustment is present is close to 2048, the value corresponding to 11-bit digitization.

Finally, the vignetting introduced by the lens, filter, and filter mount was measured experimentally for the various apertures of interest ($N=1.7$, $N=2.0$, $N=2.8$, and $N=4.0$), by registering the relative illumination data across the field
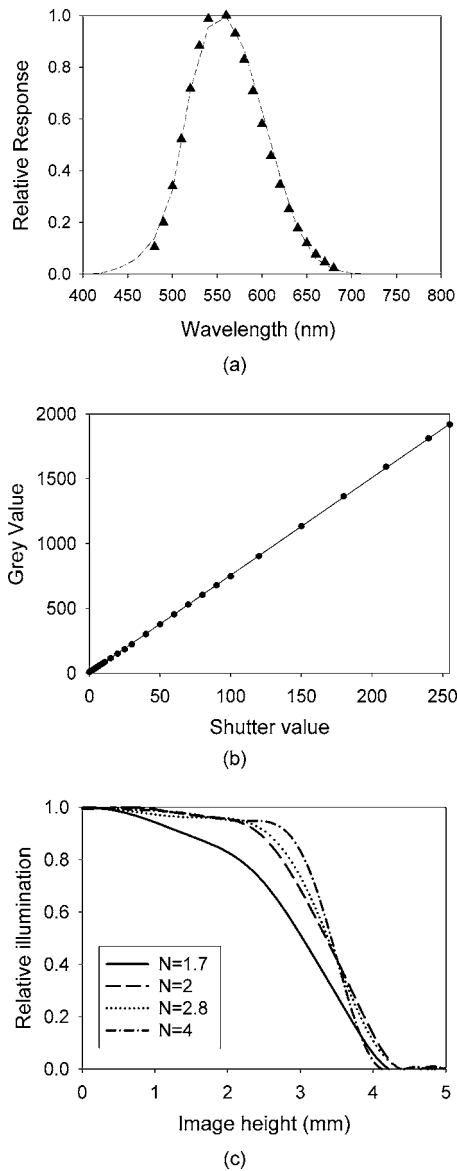
(a)

(b)

(c)

Fig. 3 Sensor calibrations: (a) spectral response of the sensor (symbols) against CIE V_λ photopic observer (line); (b) linearity of the response with external shutter control (gray level against shutter value); (c) vignetting of the sensor for different apertures when exposed to a uniform luminance field.

of view of the CCD array when the sensor was exposed to uniform illumination [Fig. 3(c)]. In order to yield a uniform transmittance across the field of view and to assign an appropriate correction factor to each pixel in the CCD, the relative illumination data measured across the array were curve-fitted, and equations for correction of vignetting effects at each aperture were obtained.

To complete the sensor, a complete Visual C++ user interface was developed, including the remote control for the motor sequence on the measurement plane, the control of register acquisitions, and the computation of the final photometric distribution, which is carried out during the measurement process to speed up the total measurement time. The measured photometric distribution at the final plane is shown graphically on the screen and saved to a text
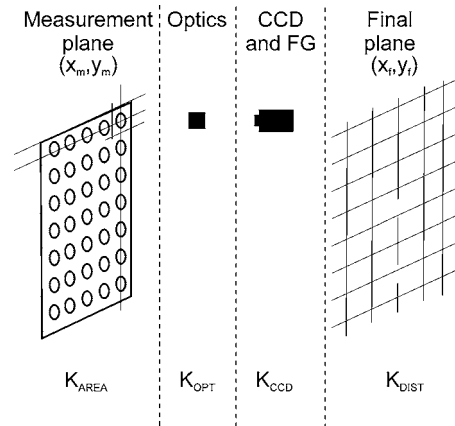

Fig. 4 Factors in the measurement chain.

file for subsequent processing, if necessary. The illumination control points outlined in ECE regulations are also highlighted graphically on the calculated photometric distribution plot for ease of use.

4 Photometric Calibration

Once the unit is able to perform the measurement of far-field photometric distributions from near-field data, the last step is to obtain the relation of the gray-level data accumulated on the final plane to real-world photometric units. This task has been addressed using a simple theoretical model of consecutive conversion values, by dividing the measurement chain into a number of independent stages (Fig. 4). Each of these stages was linked to a conversion, loss, or correction factor which may be analytically or empirically determined. In the next paragraphs we follow the measurement chain of our unit and present the different correction factors involved.

The first correction factor needs to be introduced to take account of the relationship between the real area covered by the aperture of the sensor (corresponding to the optics aperture) and the square area defined by the horizontal and vertical displacement steps between consecutive measurement points, as

$$K_{AREA} = \frac{\delta x \cdot \delta y}{\pi (\Phi_{PE}/2)^2}, \tag{3}$$

where δx and δy are the horizontal and vertical displacement steps in the measurement plane, and Φ_{PE} is the size of the optics entrance pupil.

As the energy enters the sensor, it is affected first by the loss factor related to the average optics transmission (K_{OPT}), which includes the effect of the neutral filters used to prevent the saturation of the image at minimum exposure. The illumination received on the CCD sensor is then affected by an additional conversion factor related to digitizing the signal and recording it in a file as a gray level (K_{CCD}), which depends on the camera and framegrabber used. Vignetting and shutter corrections are then applied to the measured gray-level distribution of image i
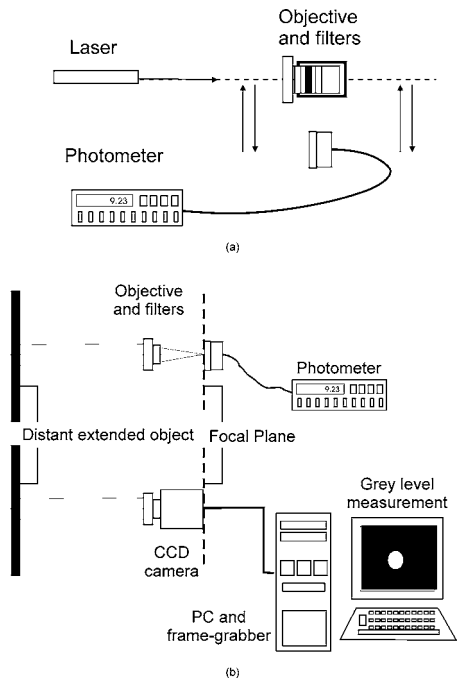
Fig. 5 Experimental setups for the measurement of (a) K_{OPT} and (b) K_{CCD}.

Table 2 Photometric calibration constants for the working conditions in Table 1. Here K_{OPT} is presented for the typical configuration involving an optical-density-3.4 neutral-density filter. All constants are dimensionless except K_{CCD}.

Constant	Value
K_{OPT}	4.169×10^5
K_{CCD}	4.455×10^{-3} (lux/gray level)
K_{AREA}	0.611
K_{DIST}	4.733×10^{-7}
K_{TOT}	5.371×10^{-5}

$$E(x_{f'}, y_f) = K_{TOTAL} \sum_{i=1}^{N} p_i(x_{CCD}, y_{CCD}), \tag{5}$$

where N is the total number of registers acquired in the near field, and

$[p_i(x_{CCD}, y_{CCD})]$ by means of the calibrations of the sensor described in Sec. 3.2, which yield the corrected gray-level value $p_i'(x_{CCD}, y_{CCD})$ for image i.

Afterwards, the corrected gray-level value of each pixel is propagated to the final plane in the proper direction, so a final correction factor K_{DIST} dependent on the propagation distance needs be introduced, expressed by

$$K_{DIST} = \frac{f'^2}{d_{M-F}^2}, \tag{4}$$

where f' is the focal length of the camera lens and d_{M-F} is the distance from the measurement plane to the final plane. The accumulated illumination value at a given pixel in the final plane may then be obtained through

Table 1 Typical experimental conditions for the sensor.

Parameter	Value
δx	7.0 mm
δy	7.0 mm
ϕ_{PE}	10.1 mm
f'	17.2 mm
d_{M-F}	25.0 mm

Fig. 6 Headlamps used for experimental results: (a) asymmetrical; (b) symmetrical.
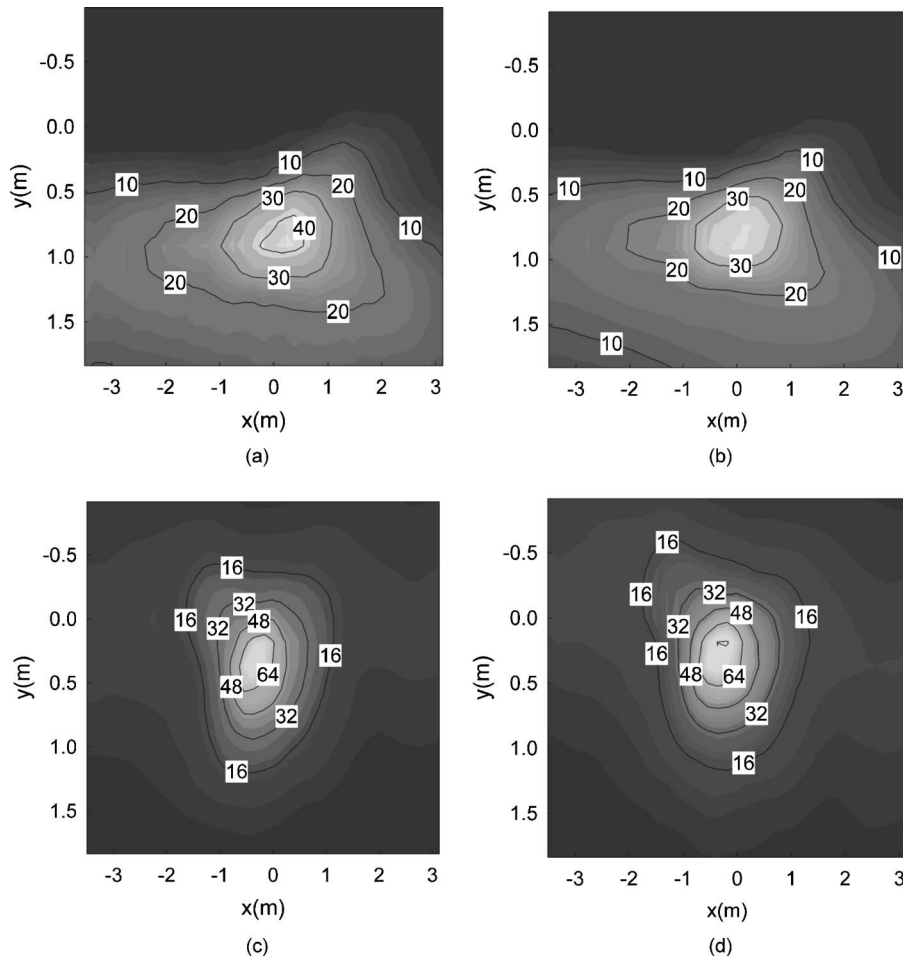
Fig. 7 Results for asymmetrical headlamp: (a) passing beam, measured; (b) passing beam, reference; (c) driving beam, measured; (d) driving beam, reference.

$$K_{\text{TOTAL}} = K_{\text{OPT}} K_{\text{CCD}} K_{\text{DIST}} K_{\text{AREA}} . \qquad (6)$$

This means that all the factors are known except the average optics transmission (K_{OPT}) and the flux to gray-level conversion of the CCD camera and framegrabber (K_{CCD}), which were measured using the simple experimental setups presented in Fig. 5. Here K_{OPT} is determined by comparing the average responses of a calibrated International Light IL-1700 radiometer to light before and after it passed through the optical system, including optics, neutral-density, and spectral filters [Fig. 5(a)], and K_{CCD} is determined from the comparison of the sum of gray levels obtained when imaging a distant extended object acquired through the sensor with the response of the calibrated radiometer when placed at the focal plane of the CCD. The correct positioning of the radiometer is ensured by the use of an autocollimator [Fig. 5(b)]. It should be emphasized that this procedure allows the conversion factors from the sensor and the framegrabber to be determined simultaneously as a single value. Typical working conditions for the unit are presented in Table 1. The corresponding values for the different calibration constants under the working conditions of Table 1 are listed in Table 2.

When using working conditions different from those presented in this paper, the factors corresponding to steps in

the measurement chain affected by the new working conditions need to be measured or calculated following the same procedures or expressions detailed next, so the calibration procedure is general, although it has been presented for the particular working conditions described in Table 1. For instance, changes in the scanning strategy would only affect K_{AREA}, which would be recalculated while the remaining factors leading to K_{TOTAL} would remain constant.

5 Results

Results are presented for two different types of headlamps used in commercial automotive units under different illumination conditions. One of them is a modern headlamp with a periodic pattern on the reflector and a completely transparent cover, which corresponds to a commercial asymmetrical right-driving headlamp [Fig. 6(a)]. The other is a symmetrical headlamp of a simpler, more classic design involving a smooth reflector and an array of small prismatic lenslets in the cover [Fig. 6(b)]. Both headlamps were tested under passing-beam and driving-beam conditions.

The results obtained using the unit are compared with the distributions of the same headlamps measured in a reference photometric tunnel at IDIADA (L'Albornar, Tarra-
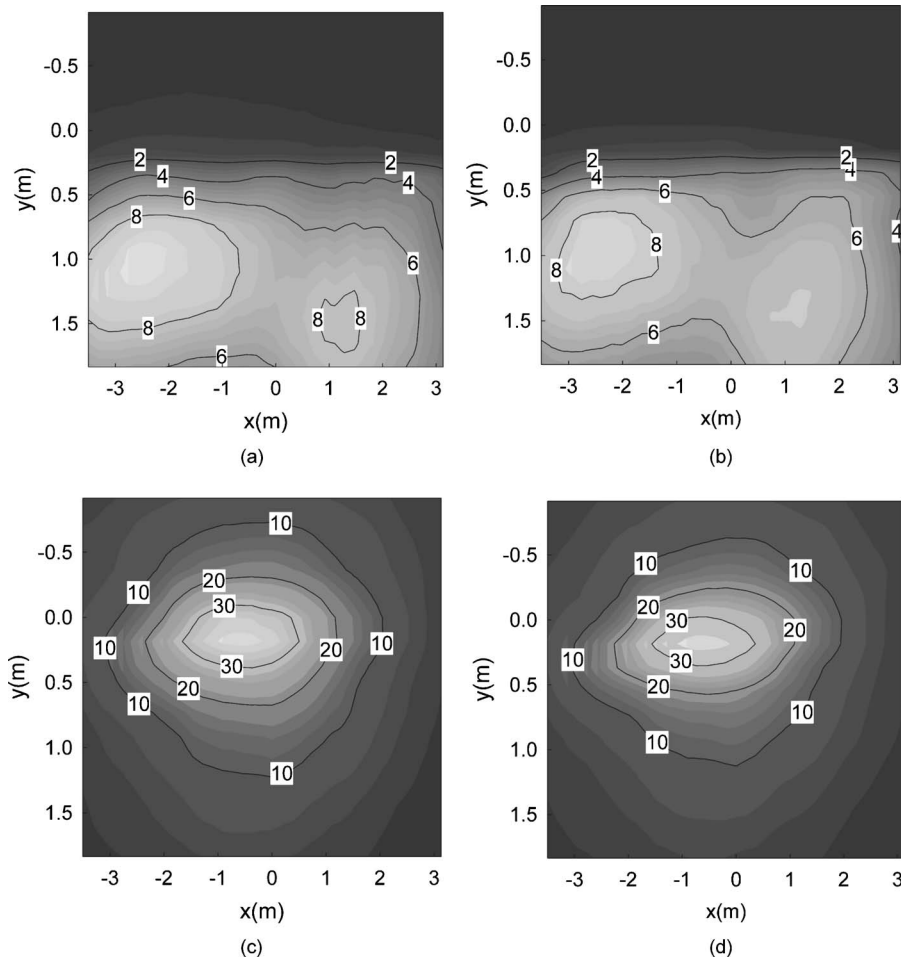
Fig. 8 Results for symmetrical headlamp: (a) passing beam, measured; (b) passing beam, reference; (c) driving beam, measured; (d) driving beam, reference.

gona, Spain). The lamps for both headlamps were calibrated using an integrating sphere to yield flux emission according to the regulations. The measurements in the photometric tunnel involved the custom programming of the goniometer position to measure an array of 51×31 data points, large enough to compare the photometric distributions obtained; the usual photometric tunnel testing procedure is confined to the small number of control points specified in the regulations. In our unit, measurements were arranged to divide the final plane into an array of 256 $\times 256$ cells, of size 33×33 mm each. The minimum spatial resolution value that may be attained on the final plane, however, corresponds to the projected size of the pixel of the camera, which has a value of 15 mm under these working conditions. The measurement time in the photometric tunnel was 40 min, while our unit performed the complete photometric distribution in 12 min with a much larger number of data points. This is due to the simultaneous energy sensing enabled by the pixels in the CCD array.

Figures 7 and 8 compare driving- and passing-beam measurements with the unit in the photometric tunnel for both headlamps. The measured and reference distributions are very close in all cases, with relative errors below 10% in the bright areas in all distributions. We have thus shown how the simple and low-cost measurement strategy pro-

posed yields reliable and quick results in the measurement of photometric distributions in far-field conditions from near-field measurements, both for complex and for simple headlamp shapes. The approach may easily be extended to other sources, such as luminaires, provided the aperture of the lens can adequately cope with the aperture of the rays coming out of the source.

6 Conclusions

A simple and cost-effective strategy for light source testing is described and applied to automotive headlamps. Measurements taken with a calibrated CCD camera in a number of points at a plane close to the source allow the measurement of the direction and amount of energy in the near field. This information enables the final distribution on a surface at any distance to be computed, although the results presented are for a plane placed 25 m away from the headlamp, as described in automotive regulations. The results for an asymmetrical and a symmetrical headlamp in passing- and driving-beam conditions are compared with those obtained in a photometric tunnel, showing very good agreement. The relative error in the bright areas of the dis-

tribution stays within 10%, while the measurement times are much shorter than the equivalent ones for a photometric tunnel.

References

1. J. Moisel, "Solid state night vision systems," *Proc. SPIE* **5663**, 47–54 (2004).
2. J. Lonnoy, Y. Le Guilloux, and R. Moreira, "Far IR vision cameras for automotive safety," *Proc. SPIE* **5663**, 156–169 (2004).
3. Economic Commission for Europe (ECE), "Regulation N112: motor vehicle headlamps emitting an asymmetrical passing beam or a driving beam or both and equipped with filament lamps," http://www.unece.org/trans/main/wp29/wp29regs101-120.html (2001).
4. Economic Commission for Europe (ECE), "Regulation N113: motor vehicle headlamps emitting a symmetrical passing beam or a driving beam or both and equipped with filament lamps," http://www.unece.org/trans/main/wp29/wp29regs101-120.html(2001).
5. SAE Recommended Practice, "Harmonized vehicle headlamp performance requirements," SAE J1735 JAN95, 122-24 (1995).
6. K. Ohana, "Illuminance measurement of vehicle lamp," U. S. Patent No. 5,426,500 (1995).
7. T. Vernon, "Measurement of the output of a lamp," G. B. Patent No. 2,275,333 (1994).
8. J. Arasa, S. Royo, and C. Pizarro, "Profilometry of toroidal surfaces with an improved Ronchi test," *Appl. Opt.* **39**, 5721–5731 (2000).
9. I. Lewin, R. Laird, and J. Young, "The application of video camera techniques to photometry," *J. Illum. Eng. Soc.* **20** 316–322 (1991).
10. J. R. Janesick, *Scientific Charge-Coupled Devices*, SPIE Press (2001).
11. C. De Cusatis, *Handbook of Applied Photometry*, Am. Inst. of Physics, New York (1992).

Santiago Royo completed his PhD in applied optics at 1999 at the Technical University of Catalonia, where he teaches optical technology and ophthalmic lenses. He is also a senior researcher in the Center for Sensor, Instrumentation and Systems Development. His research interests involve optical metrology and fabrication topics, photometric testing, and adaptive optics.

María Jesús Arranz completed her BSc degree in physics at the University of Barcelona in 1999. From 1999 to 2005 she was a teaching assistant at the Technical University of Catalonia. At present she is working as a researcher in Optical Engineering at the Center for Sensor, Instrumentation and Systems Development. Her work focuses on optical measurement techniques. She is currently pursuing her PhD degree.

Josep Arasa. He received his BSc in physics from Universitat de Barcelona in 1980 and his PhD in physical sciences from Universitat de Barcelona in 1988. He joined the School of Optics and Optometry of the Technical University of Catalonia in 1983 as an assistant lecturer, and later became a lecturer (1987), then a professor (1992). From the beginning of his career, he has been involved in optical design and optical metrology. His research themes concern industrial applications of vision and optoelectronics metrology.

Michel Cattoen received his PhD from Université Paul Sabatier in 1975, and his Doctorate of Sciences degree from the National Polytechnic Institute of Toulouse (INPT) in 1985. He joined the engineering school ENSEEIHT in 1974 as a research assistant; there he became first a lecturer (1986) and then a professor (1990). He is presently a second-class professor in the same institution. From the beginning of his career, he has been involved in television and image processing, mainly in industrial applications (computer vision). His research themes concern applications in industrial vision and optoelectronic metrology.

Thierry Bosch received his PhD from the National Institute of Applied Science of Toulouse (INSAT) in 1992. He was the head of a group on optoelectronics, instrumentation, and sensors from 1993 to 2000. He is presently a second-class professor in the engineering school ENSEEIHT of Toulouse, and director of the electronics laboratory of ENSEEIHT (LEN7). His research interests are related to laser industrial instrumentation development, including interferometry, phase-shift and self-mixing-based range-finding techniques, and vibration and velocity measurements.